Ubiquitination of the PI3-kinase VPS-34 promotes VPS-34 stability and phagosome maturation

Jinchao Liu,[1,2,3,5] Meijiao Li,[3] Lin Li,[1] She Chen,[1] and Xiaochen Wang[1,2,3,4,5]

[1]National Institute of Biological Sciences and [2]Chinese Academy of Medical Sciences, Beijing, China
[3]National Laboratory of Biomacromolecules, Chinese Academy of Sciences Center for Excellence in Biomacromolecules, Institute of Biophysics, Chinese Academy of Sciences, Beijing, China
[4]College of Life Sciences, University of Chinese Academy of Sciences, Beijing, China
[5]Peking Union Medical College, Beijing, China

Apoptotic cells generated by programmed cell death are engulfed by phagocytes and enclosed within membrane-bound phagosomes. Maturation of apoptotic cell–containing phagosomes leads to formation of phagolysosomes where cell corpses are degraded. The class III phosphatidylinositol 3-kinase (PI3-kinase) VPS-34 coordinates with PIKI-1, a class II PI3-kinase, to produce PtdIns3P on phagosomes, thus promoting phagosome closure and maturation. Here, we identified UBC-13, an E2 ubiquitin–conjugating enzyme that functions in the same pathway with VPS-34 but in parallel to PIKI-1 to regulate PtdIns3P generation on phagosomes. Loss of *ubc-13* affects early steps of phagosome maturation, causing accumulation of cell corpses. We found that UBC-13 functions with UEV-1, a noncatalytic E2 variant, and CHN-1, a U-box–containing E3 ubiquitin ligase, to catalyze K63-linked poly-ubiquitination on VPS-34 both in vitro and in *Caenorhabditis elegans*. Loss of *ubc-13*, *uev-1*, or *chn-1* disrupts ubiquitin modification of VPS-34 and causes significantly reduced VPS-34 protein levels. Our data suggest that K63-linked ubiquitin modification serves as a general mechanism to modulate VPS-34 stability in multiple processes.

Introduction

Phagocytic removal of apoptotic cells is important for preventing autoimmune responses and maintaining tissue homeostasis. In *Caenorhabditis elegans* hermaphrodites, 131 somatic cells and up to half of the germ cells undergo apoptosis, and the resulting cell corpses are quickly removed by neighboring cells in the soma or by gonadal sheath cells that encase the germline. Upon recognition, apoptotic cells are internalized by phagocytes and enclosed within membrane-bound vesicles, namely phagosomes (Pinto and Hengartner, 2012; Wang and Yang, 2016). Phagosome scission separates the vesicle from the plasma membrane to complete engulfment and initiate a maturation process. Maturation of cell corpse–enclosing phagosomes involves sequential interactions with early endosomes, late endosomes, and lysosomes to generate phagolysosomes where apoptotic cells are degraded (Pinto and Hengartner, 2012; Wang and Yang, 2016). Two lipid kinases, VPS-34, a class III phosphatidylinositol 3-kinase (PI3-kinase), and PIKI-1, a class II PI3-kinase, act coordinately to produce PtdIns3P on phagosomes, which is important for both phagosome closure and maturation (Wang and Yang, 2016). Loss of both VPS-34 and PIKI-1 almost completely blocks PtdIns3P generation on phagosomes and causes more severe cell corpse removal

defects than either of the single mutants (Zou et al., 2009; Lu et al., 2012; Cheng et al., 2013). PIKI-1 associates with extending pseudopods and nascent phagosomes, where it acts with the PtdIns3P phosphatase MTM-1 to control PtdIns3P levels for phagosome sealing (Cheng et al., 2015). VPS-34 contributes to PtdIns3P generation at the sealing stage but plays a major role in producing PtdIns3P on fully sealed phagosomes (Cheng et al., 2015). PtdIns3P, which transiently accumulates on sealed phagosomes, controls early maturation events by recruiting PtdIns3P-binding effectors, leading to degradation of apoptotic cells (Chen et al., 2010; Pinto and Hengartner, 2012; Wang and Yang, 2016). It is unclear, however, whether and how VPS-34 is regulated in cell corpse clearance.

In addition to removing cell corpses, the class III PI3-kinase VPS-34 also controls other PtdIns3P-mediated processes such as endosome maturation and autophagy. In these processes, Vps34 is assembled into tetrameric complexes with Vps15, Vps30/Beclin 1 and Atg14 to regulate autophagy or with Vps15, Vps30/Beclin 1 and Vps38/UVRAG to control vesicular trafficking (Kihara et al., 2001; Itakura et al., 2008). The lipid kinase activity and membrane recruitment of Vps34 require Vps15, whereas assembly of tetrameric complexes further enhances Vps34 activity (Backer, 2016). The presence
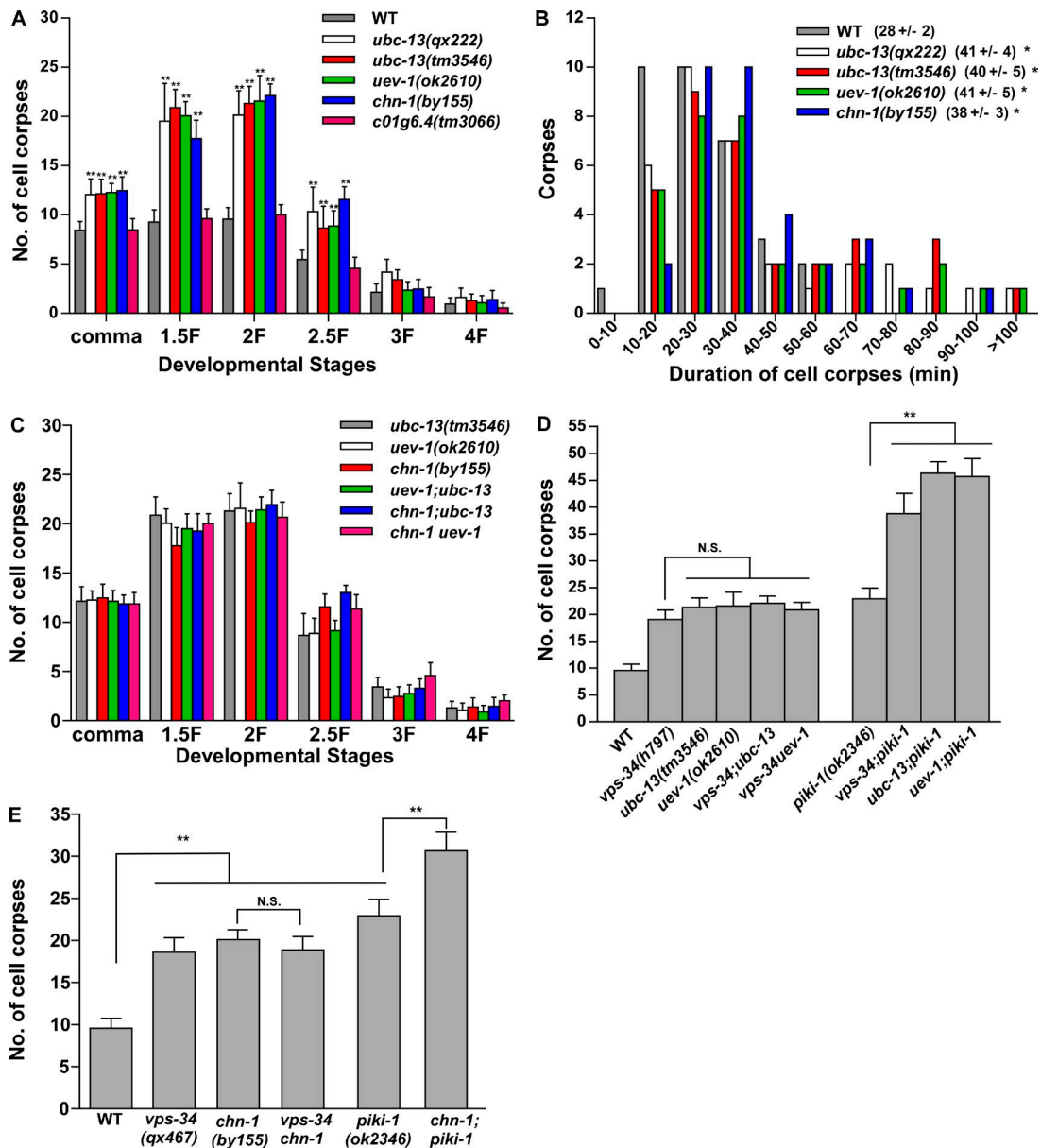
Figure 1. **Loss of *ubc-13*, *uev-1*, or *chn-1* affects cell corpse removal.** (A and C) Time course analysis of cell corpse appearance during embryonic development was performed in the indicated strains. At least 15 embryos were scored at each stage in each strain. Data are shown as mean ± SD. Data derived from different genetic backgrounds at multiple developmental stages were compared by two-way ANOVA followed by Bonferroni posttest. Mutant datasets were compared with WT (A), and datasets from double mutants were compared with single mutants (C). **, P < 0.001; all other points, P > 0.05. (B) Four-dimensional microscopy analysis of cell corpse duration was performed in WT, *ubc-13(qx222)*, *ubc-13(tm3546)*, *uev-1(ok2610)*, and *chn-1(by155)*. The persistence of 33 cell corpses from three embryos in each strain was monitored. The mean duration (± SEM) is shown in parenthesis. The Kaplan-Meier method followed by the log-rank test was performed to compare mutant datasets with WT. *, P < 0.05. (D and E) Cell corpses were scored at the twofold embryonic stage in the indicated strains. At least 15 embryos were scored in each strain. Data are shown as mean ± SD. One-way ANOVA with Tukey's posttest was performed to compare datasets that are linked by lines. **, P < 0.0001; N.S., no significance.

of Vps34/VPS34 appears to be important for stabilization of Vps15, Beclin 1, ATG14, and UVRAG, suggesting that Vps34 is important for the stability of other complex members (Kihara et al., 2001; Itakura et al., 2008; Thoresen et al., 2010). In addition, multiple ubiquitin-mediated regulation pathways are found to affect the stability or scaffold function of Beclin 1 (Reidick et al., 2014; Backer, 2016). In contrast, much less is known about how Vps34 stability is regulated. In HeLa cells, depletion of VPS15 appears to reduce the levels of other complex members including VPS34 (Thoresen et al., 2010). The ubiquitin ligase Cul3-KLHL20 is reported to mediate

degradation of ULK1, Beclin 1, and VPS34 during prolonged starvation to restrain autophagy (Liu et al., 2016). In response to DNA damage, the FBX120–Skp1–Cullin1 complex mediates ubiquitination and proteasomal degradation of Vps34, leading to inhibition of autophagy and receptor endocytosis (Xiao et al., 2015). Nevertheless, it is unknown whether Vps34 stability may be protected by ubiquitin-mediated regulatory pathways under basal or stress conditions.

Ubc13 is an E2 ubiquitin–conjugating enzyme that functions with noncatalytic E2-like partner proteins Mms2 or Uev1A to mediate K63-linked poly-ubiquitination of a variety

of substrates (Hodge et al., 2016). Ubc13 participates with different E3 ubiquitin ligases in diverse cellular processes such as inflammatory and DNA damage response pathways and endocytosis of membrane proteins (Hodge et al., 2016). For example, Ubc13 interacts with CHIP, a U-box–containing E3 ligase, to regulate endocytosis of growth hormone receptor (Slotman et al., 2012). In *C. elegans*, UBC-13 is important for clearance of maternal membrane proteins by catalyzing K63-linked ubiquitination (Sato et al., 2014). Neither Ubc13/UBC-13 nor CHIP/CHN-1 has been found to regulate Vps34 or Vps34 complexes.

In this study, we identify UBC-13 as a novel regulator of cell corpse clearance. UBC-13 functions in the same pathway with VPS-34 but in parallel to PIKI-1 to promote PtdIns3P generation on apoptotic cell–containing phagosomes. We found that UBC-13 acts with UEV-1, a noncatalytic E2 variant, and CHN-1, a U-box–containing E3 ubiquitin ligase, to catalyze K63-linked poly-ubiquitination of VPS-34, and thus promotes VPS-34 stability. Our data reveal a novel ubiquitin-mediated regulatory mechanism that protects VPS-34 stability. Expression of human UBE2N/Ubc13 can substitute for UBC-13 function in removing cell corpses, indicating conserved roles of Ubc13 in this process.

Results

Loss of UBC-13 and UEV-1 affects apoptotic cell clearance through phagosome maturation

We isolated *qx222* from a forward genetic screen for animals that contain significantly more cell corpses than WT at various embryonic stages (Fig. 1 A). Cell corpses persisted significantly longer in *qx222* mutants than in WT, suggesting that cell corpse removal is defective in *qx222* (Fig. 1 B). We found that *qx222* affects the gene *ubc-13*, which encodes an E2 ubiquitin–conjugating enzyme that is well conserved across yeast, worms, and humans (Fig. S1, A and B). *tm3546*, a deletion mutation of *ubc-13* that results in a truncated protein containing only the first 87 amino acids, exhibited a similar cell corpse phenotype as in *qx222* (Fig. 1, A and B; and Fig. S1 A). Expression of UBC-13 or UBE2N, the human homologue of UBC-13, efficiently rescued the cell corpse phenotype in *qx222* or *tm3546* (Fig. S1, C and D). Collectively, these data indicate that loss of UBC-13 affects apoptotic cell clearance, and human UBE2N can substitute for worm UBC-13 in removing cell corpses.

The ubiquitin-conjugating enzyme Ubc13 forms heterodimers with the noncatalytic E2-variant Uev1 to mediate K63-linked poly-ubiquitination of a variety of substrates (Hodge et al., 2016). We found that loss of *uev-1* function, caused by a deletion mutation *ok2610*, led to increased numbers and extended duration of cell corpses like in *ubc-13(lf)* mutants, and this cell corpse phenotype was unaltered in *uev-1;ubc-13* double mutants (Fig. 1, A–C). These data indicate that UBC-13 and UEV-1 act together to promote apoptotic cell clearance.

Cell corpses in *ubc-13(tm3546)* and *uev-1(ok2610)* were surrounded by the phagocytic receptor CED-1 as in WT, suggesting that recognition and initiation of engulfment are not affected (Fig. 2, A–B′ and Q). However, phagosomal association of RAB-5 and the PtdIns3P biosensor 2xFYVE, which both appear at the early stage of phagosome maturation, was reduced significantly in *ubc-13(tm3546)* and *uev-1(ok2610)* (Fig. 2, D–E′, M–O′, Q, and R). Moreover, the signals from the late phagosome marker RAB-7 and the lysosomal membrane protein LAAT-1 were also greatly decreased on phagosomes in *ubc-13(tm3546)* and *uev-1(ok2610)* mutants (Fig. 2, G–H′, J–K′, and Q). These data suggest that loss of *ubc-13* and *uev-1* impairs phagosome maturation at an early stage.

CHN-1 is the UBC-13–interacting E3 that promotes phagosome maturation

We performed a yeast-two-hybrid (Y2H) screen to search for UBC-13–interacting E3 ubiquitin ligases that function with UBC-13 and UEV-1 to promote apoptotic cell clearance. We identified several UBC-13–interacting proteins by Y2H screening including CHN-1, an E3 ubiquitin ligase that is homologous to human CHIP (C-terminal Hsp70 interacting protein). CHN-1 interacted with UBC-13 in yeast cells, and recombinant CHN-1 protein was efficiently pulled down by GST–UBC-13 but not GST, indicating that CHN-1 directly interacts with UBC-13 (Fig. 3, A–C). The U-box domain of CHN-1, but not the tetratricopeptide repeat (TPR) domain or the helical domain, was sufficient to bind UBC-13, whereas mutations in the conserved E3-binding SPA (serine-proline-alanine) motif of UBC-13 completely abolished the interaction between UBC-13 and CHN-1 (Fig. 3, A–C; and Fig. S1 B; Campbell et al., 2012). These data indicate that the CHN-1–UBC-13 interaction is mediated by the U-box domain of CHN-1 and the SPA motif of UBC-13. *by155* and *tm2692* are two deletion mutations of *chn-1* that are predicted to create truncated CHN-1 proteins that lack the U-box domain and TPR domain, respectively (Fig. S1 E; Hoppe et al., 2004). Both *by155* and *tm2692* embryos contained increased numbers of apoptotic cells, and cell corpses persisted significantly longer in *chn-1(by155)* than in WT, suggesting that cell corpse removal is defective in *chn-1(lf)* mutants (Fig. 1, A and B; and Fig. S1 F). In contrast, loss of C01G6.4, a UBC-13–interacting E3 ligase homologous to human RNF11 identified from the Y2H screen, did not affect cell corpse clearance in WT, *ubc-13(tm3546)*, or *chn-1(by155)*, indicating that it is dispensable for cell corpse clearance (Fig. 1 A and Fig. S1, G and H). The *chn-1(by155)* mutant exhibited cell corpse phenotypes identical to those in the *ubc-13(tm3546)* and *uev-1(ok2610)* single mutants, and the *chn-1;ubc-13* or the *chn-1;uev-1* double mutants (Fig. 1 C). Moreover, phagosomal association of RAB-5, PtdIns3P, RAB-7, and LAAT-1 was significantly reduced in *chn-1(by155)* mutants like in *ubc-13(tm3546)* and *uev-1(ok2610)* worms, suggesting that loss of *chn-1* impairs phagosome maturation (Fig. 2, A–Q). Collectively, these data indicate that UBC-13, UEV-1, and CHN-1 function together to promote apoptotic cell clearance through phagosome maturation.

UBC-13–UEV-1–CHN-1 acts in the same pathway with VPS-34 to promote phagosome maturation

PtdIns3P was significantly reduced on phagosomes in *ubc-13(lf)*, *uev-1(lf)*, and *chn-1(lf)* mutants, suggesting that UBC-13, UEV-1, and CHN-1 may be involved in regulating PtdIns3P generation or its turnover on phagosomes. The class III and class II PI3-kinases VPS-34 and PIKI-1 act coordinately to control PtdIns3P generation on phagosomes (Zou et al., 2009; Lu et al., 2012; Cheng et al., 2013, 2015). Loss of both VPS-34 and PIKI-1 almost completely blocked PtdIns3P generation on phagosomes and caused more severe cell corpse removal defects than either of the single mutants (Fig. 1 D; Fig. 2, R and S; and Fig. S2 A; Zou et al., 2009; Lu et al., 2012; Cheng et al., 2013).
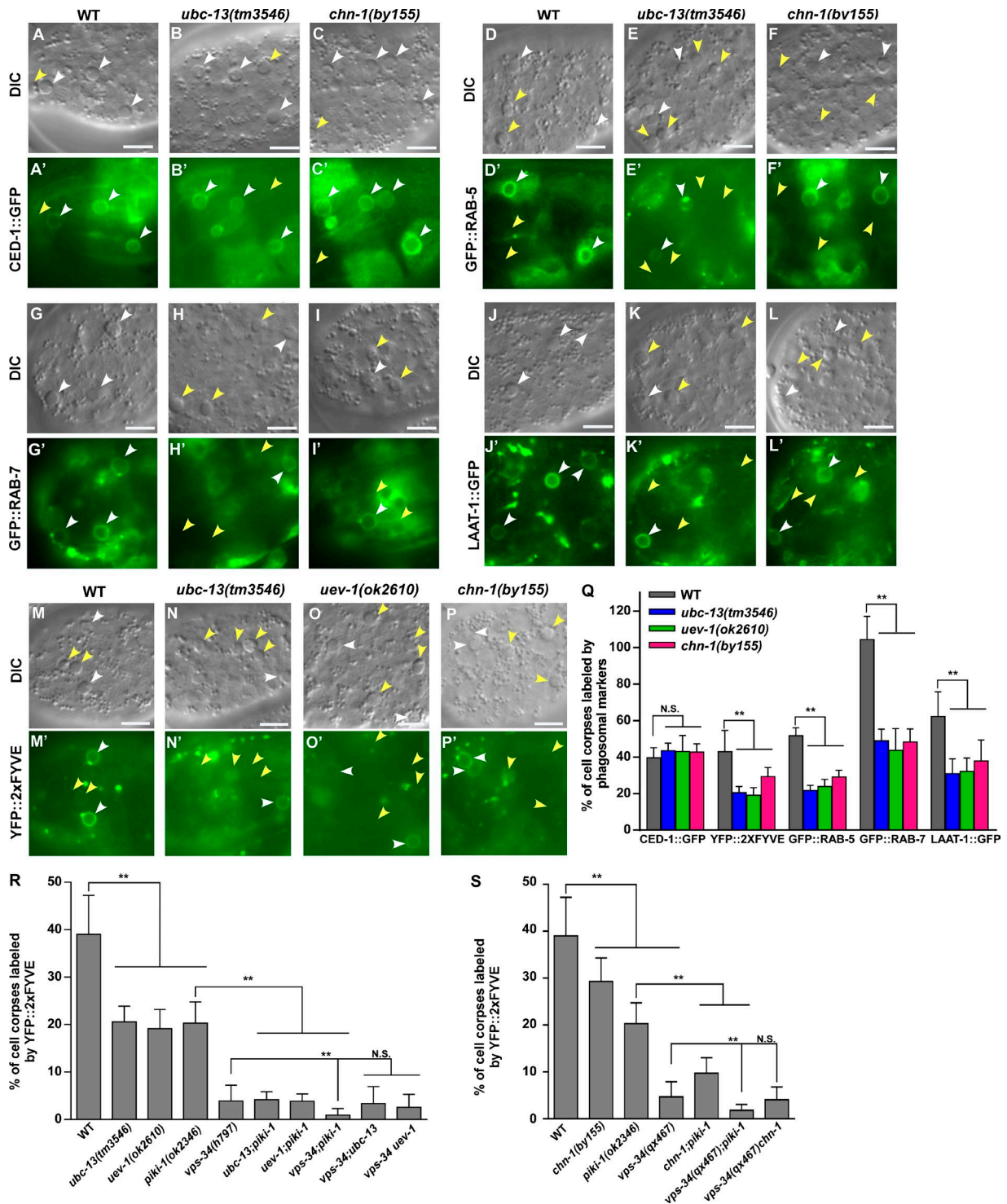
Figure 2. **UBC-13, UEV-1, and CHN-1 act in the same pathway with VPS-34 to regulate phagosome maturation.** (A–P) DIC and fluorescent images of cell corpses in the indicated strains expressing CED-1::GFP (A–C), GFP::RAB-5 (D–F), GFP::RAB-7 (G–I), LAAT-1::GFP (J–L), and YFP::2xFYVE (M–P). The head region of embryos at the twofold stage is shown. Cell corpses labeled by fluorescent markers are indicated by white arrowheads and unlabeled corpses are indicated by yellow arrowheads. Bars, 5 µm. (Q) The percentage of cell corpses labeled by phagosomal markers shown in A–L was quantified. (R and S) The percentage of cell corpses labeled by YFP::2XFYVE was quantified in the indicated strains. In Q–S, at least 15 embryos were scored in each strain. Data are shown as mean ± SD. One-way ANOVA with Tukey's posttest was performed to compare mutant datasets with WT (Q) or datasets linked by lines (R and S). **, P < 0.0001; N.S., no significance.

Mutations in BEC-1 or VPS-15 caused an increased number of cell corpses, as in *vps-34(lf)* mutants, and this phenotype was further enhanced by *piki-1(lf)* (Fig. S2 D), consistent with BEC-1, VPS-15, and VPS-34 acting in a complex. We found that

loss of *ubc-13* or *uev-1* significantly increased the cell corpse numbers in *piki-1(lf)* mutants but not in *vps-34(lf)* or *bec-1(lf)* mutants (Fig. 1 D and Fig. S2, A–C). Moreover, loss of *ubc-13*, *uev-1*, or *piki-1* caused a similar reduction in phagosomal
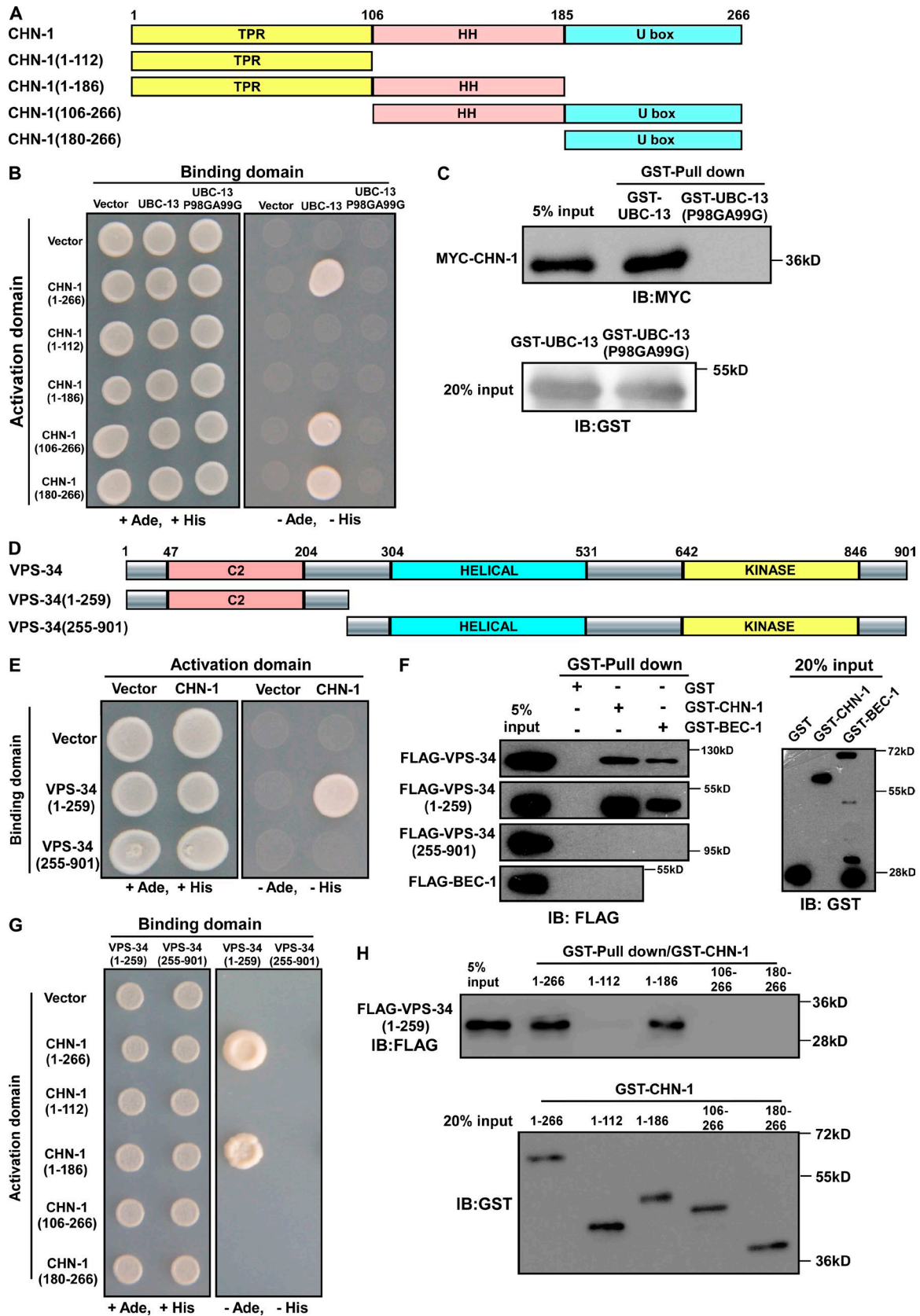
Figure 3. **CHN-1 interacts with UBC-13 and VPS-34.** (A and D) Schematic diagram showing domains and truncations of CHN-1 (A) and VPS-34 (D), which were used to examine CHN-1–UBC-13 and CHN-1–VPS-34 interactions. (B, C, and E–H) The interaction between CHN-1 and UBC-13 (B and C), and CHN-1 and VPS-34 (E–H), were examined by yeast two-hybrid analyses (B, E, and G) and GST pulldown assays (C, F, and H). IB, immunoblot. The CHN-1–UBC-13 interaction occurs through the U-box domain of CHN-1 (B) and the SPA motif of UBC-13 (B and C). The CHN-1–VPS-34 interaction is mediated by the C2 domain of VPS-34 (E and F) and the TPR and helical (HH) domains of CHN-1 (G and H).

PtdIns3P, which was further reduced in *ubc-13(lf);piki-1(lf)* and *uev-1(lf);piki-1(lf)* double mutants (Fig. 2 R). The *ubc-13* mutation also led to a further reduction in phagosomal labeling by RAB-5, RAB-7, and LAAT-1 in *piki-1(lf)* mutants (Fig. S2, E–G). In contrast, loss of *piki-1* but not *ubc-13* or *uev-1* caused a further reduction in PtdIns3P on phagosomes in *vps-34* mutants (Fig. 2 R). Collectively, these data indicate that UBC-13 and UEV-1 function in the same pathway with VPS-34 but in parallel to PIKI-1 to promote phagosome maturation and cell corpse degradation.

We were unable to construct *vps-34 chn-1* double mutants because the genes are located very close together on linkage group I. To solve this, we generated a mutant allele of *vps-34* by CRISPR-Cas9 in both WT and *chn-1(by155)* worms, which led to a premature stop codon at the N-terminus of VPS-34 (Fig. S4 A). Animals carrying the resulting *vps-34* mutant allele, *qx467*, contained significantly more cell corpses than WT (Fig. S2 D). The *qx467* phenotype resembled that of *h797* mutants, which carry a strong loss-of-function allele of *vps-34*, and also of *bec-1(ok700)* and *vps-15(qx525)* mutants (Fig. S2 D). We found that loss of *chn-1* enhanced the cell corpse phenotype of *piki-1(ok2346)* but not *vps-34(qx467)* or *bec-1(ok700)* mutants (Fig. 1 E and Fig. S2 C). Loss of *chn-1* did not affect PtdIns3P accumulation in *vps-34(qx467)* phagosomes but caused further reduction in phagosomal PtdIns3P, RAB-5, RAB-7, and LAAT-1 in *piki-1(ok2346)* mutants (Fig. 2 S and Fig. S2, E–G). Altogether, these data indicate that UBC-13, UEV-1, and CHN-1 function in the same pathway with VPS-34 but in parallel to PIKI-1 to promote cell corpse clearance through phagosome maturation.

Loss of UBC-13 and CHN-1 partially impairs autophagy

The class III PI3-kinase VPS-34 promotes autophagosome formation by producing PtdIns3P. The *C. elegans* Atg8/LC3 homologue LGG-1 associates with autophagosome membranes and their precursors, and is essential for autophagosome biogenesis (Tian et al., 2010). LGG-1 is mostly diffuse in WT worms but accumulates as puncta in autophagy-defective mutants (Tian et al., 2010; Lu et al., 2011). We found that GFP::LGG-1, a single-copy reporter generated by CRISPR-Cas9, formed few puncta in WT but accumulated at significantly higher levels in *ubc-13(tm3546)*, *chn-1(by155)*, and *vps-34(qx467)* mutants, suggesting that the autophagy process is affected (Fig. S3, A–C, E, and K). Loss of *piki-1* caused a similar increase in GFP::LGG-1 as in *ubc-13(lf)* or *chn-1(lf)*, but it did not further enhance the GFP::LGG-1 phenotypes in *ubc-13*, *chn-1*, or *vps-34* mutants (Fig. S3, F–K). This is in agreement with our previous finding and suggests that VPS-34 but not PIKI-1 plays a major role in autophagy (Wu et al., 2014). Autophagy activity is required for the survival of newly hatched L1 larvae in the absence of food (Kovacs and Zhang, 2010). We found that loss of *ubc-13*, *uev-1*, or *vps-34* affected the survival of starved L1 larvae, causing significantly reduced mean lifespan compared with in WT (Fig. S3 L). Collectively, these data suggest that loss of *ubc-13* and *chn-1* function impairs autophagy.

UBC-13–UEV-1–CHN-1 mediates K63-linked poly-ubiquitination of VPS-34

We next investigated whether UBC-13 (E2), UEV-1 (E2 variant), and CHN-1 (E3) catalyze ubiquitin modification of VPS-34 to regulate PtdIns3P generation. We found that VPS-34

interacted with CHN-1, the E3 ubiquitin ligase, in yeast cells, and recombinant VPS-34 but not BEC-1 was pulled down by GST–CHN-1 but not GST (Fig. 3, D–F). The C2 domain but not the core domain (helical + kinase) of VPS-34 was sufficient to bind CHN-1, whereas both the TPR and helical domains of CHN-1 were required for its interaction with VPS-34 (Fig. 3, A and D–H). These data indicate that the VPS-34–CHN-1 interaction occurs through the C2 domain of VPS-34 and the TRP and helical domains of CHN-1.

We next tested whether UBC-13–UEV-1–CHN-1 catalyzes poly-ubiquitination of VPS-34. We incubated recombinant FLAG–VPS-34 or FLAG–BEC-1 with UBA-1 (E1), UBC-13 (E2), UEV-1 (E2 variant), CHN-1 (E3), and HA-ubiquitin, then performed FLAG immunoprecipitation (IP) and detected ubiquitinated proteins using anti-HA antibodies. We found that VPS-34 but not BEC-1 was poly-ubiquitinated by UBA-1–UBC-13–UEV-1–CHN-1 (Fig. 4 A). The poly-ubiquitination of VPS-34 was completely abolished when UBC-13 or CHN-1 was removed or when only the core domain of VPS-34 (255–901), which fails to interact with CHN-1, was used (Fig. 4, A and B). Absence of the E2 variant UEV-1 led to mono- instead of poly-ubiquitination of VPS-34, consistent with the role of E2 variant in building ubiquitin chains with Ubc13 (Fig. 4, A and C). We found that inclusion of K63R- but not K48R-ubiquitin abolished the poly-ubiquitination of VPS-34, indicating that VPS-34 is modified by K63-linked but not K48-linked poly-ubiquitination (Fig. 4 C). Collectively, these data indicate that UBC-13, UEV-1, and CHN-1 mediate K63-linked poly-ubiquitination of VPS-34 in vitro.

We next examined whether VPS-34 is ubiquitinated in *C. elegans*. To do this, we inserted *flag*, *myc*, and *ha* tags into the endogenous *vps-34*, *bec-1*, *vps-15*, and *ubq-2* gene loci by CRISPR-Cas9 (Fig. S4, A–D). The resulting *C. elegans* strains *qx477*, *qx512*, *qx523*, and *qx473*, which carry *flag–vps-34*, *bec-1–myc*, *myc–vps-15*, and *ha–ubq-2*, respectively, contained similar numbers of cell corpses as in WT and had no effect on PtdIns3P accumulation on phagosomes, indicating that the tag insertions did not affect normal gene function in these strains (Fig. S4, E and F). In contrast, *qx525*, which carried *vps-15–myc*, had significantly increased numbers of cell corpses and impaired viability, suggesting that MYC insertion at the C-terminus of VPS-15 affects the function of the protein (Fig. S2 D and Fig. S4 D). We found that VPS-34 was immunoprecipitated by anti-FLAG antibodies from worm lysates prepared from *qx477 (flag-vps34)*;*qx473 (ha-ubq-2)* but not *qx473 (ha-ubq-2)*, indicating specific enrichment of FLAG–VPS-34 (Fig. 4 D). Anti-HA antibodies detected a smear of high–molecular mass species after FLAG IP in *qx477;qx473* but not in *qx473*, suggesting that VPS-34 is poly-ubiquitinated in worms (Fig. 4 D). We introduced *flag–vps-34* and *ha–ubq-2* into *ubc-13(tm3546)* and *chn-1(by155)* worms and found that poly-ubiquitination of VPS-34 was greatly reduced in *ubc-13(lf)* and *chn-1(lf)* mutants (Fig. 4 E). These data indicate that UBC-13, UEV-1, and CHN-1 catalyze poly-ubiquitination of VPS-34 in vitro and in *C. elegans*.

Lysine residues 348 and 352 are important for ubiquitin modification of VPS-34

We attempted to determine the lysine residues in VPS-34 that are modified by ubiquitin. Mass spectrometry identified six lysine residues that may be modified by ubiquitin in FLAG–VPS-34 after mono-ubiquitination in vitro by UBA-1–UBC-13–CHN-1
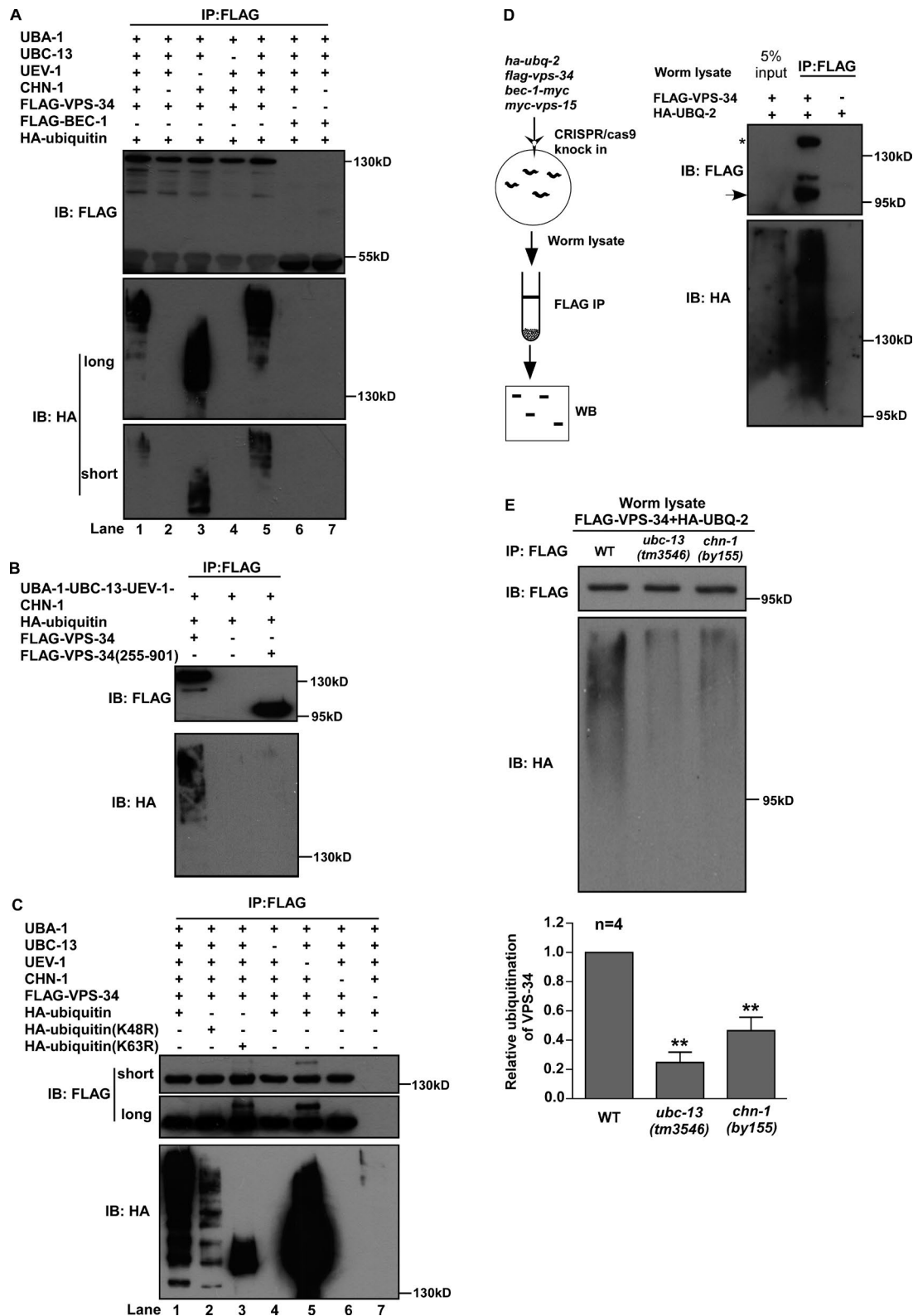
Figure 4. **UBC-13, UEV-1, and CHN-1 mediate K63-linked poly-ubiquitination of VPS-34.** (A) Ubiquitination of recombinant FLAG–VPS-34 and FLAG–BEC-1 was examined in vitro. FLAG IP was performed followed by detection of ubiquitination with anti-HA antibodies. "Long" and "short" designate long exposure time and short exposure time, respectively. Ubiquitination of VPS-34 but not BEC-1 was observed (compare lanes 1 and 5 with 6). VPS-34 ubiquitination was completely abolished when CHN-1 (lane 2) or UBC-13 (lane 4) was removed. (B) VPS-34 but not VPS-34 (255–901), which lacks the C2 domain that binds CHN-1, was ubiquitinated in vitro by UBC-13–UEV-1–CHN-1. (C) Ubiquitination of VPS-34 was examined in vitro using different forms of HA-ubiquitin (WT, K48R, and K63R). Inclusion of K63R- but not K48R-ubiquitin disrupted poly-ubiquitination of VPS-34 (compare lanes 1 and 2 with 3). "Long" and "short" designate long exposure time and short exposure time, respectively. (D) Ubiquitination of VPS-34 was examined in *C. elegans*. Schematic illustration of the ubiquitination assay is shown at the left. Worm lysates were prepared from strains generated by CRISPR-Cas9 that carry both

(Fig. S5 A). However, mutation of each individual lysine or mutation of all six lysine residues did not affect mono-ubiquitination of VPS-34 in vitro (Fig. S5 B). We next analyzed the six lysine residues in VPS-34 that were not covered by mass spectrometry analyses (Fig. S5 A). We found that mutation of lysine 348 (K348R) or lysine 352 (K352R), but not of the other four lysine residues, greatly reduced mono-ubiquitination of VPS-34 (Fig. 5 B and Fig. S5 C). K348R and K352R caused a similar reduction in poly-ubiquitination of VPS-34, which was almost completely abolished when both were mutated (Fig. 5 A). By CRISPR-Cas9, we generated *qx546*, a *vps-34* allele that contains an N-terminal FLAG tag and mutations in both lysine 348 and 352 (*flag-vps-34[K348RK352R]*; Fig. S4 A). We found that poly-ubiquitination of VPS-34 was significantly reduced in *vps-34(qx546)* compared with WT, suggesting that lysine 348 and 352 are important for the ubiquitin modification of VPS-34 in vivo (Fig. 5 C). Like *chn-1(by155)*, *vps-34(qx546)* contained increased cell corpses, and this phenotype was further enhanced in *vps-34(qx546); piki-1(ok2346)* double mutants (Fig. 5 D). Moreover, *vps-34(qx546)* caused reduced PtdIns3P on phagosomes like *chn-1(by155)*, and phagosomal PtdIns3P was further decreased in *vps-34(qx546); piki-1(ok2346)* (Fig. 5, E–H). In addition, the *vps-34(qx546)* mutation caused significantly increased GFP::LGG-1 puncta and reduced survival of L1 larvae in the absence of food, phenotypes resembling *chn-1(by155)* mutants (Fig. S3, D, K, and L). Collectively, these data indicate that poly-ubiquitination of VPS-34 is important for the function of VPS-34 in cell corpse clearance and autophagy.

Ubiquitin modification catalyzed by UBC-13–UEV-1–CHN-1 stabilizes VPS-34

We next investigated how ubiquitin modification regulates VPS-34 function. We examined VPS-34 protein levels in WT, *ubc-13(tm3546)*, and *chn-1(by155)* worms that carry *flag–vps-34* and *bec-1–myc* alleles generated by CRISPR-Cas9 (Fig. 6 A). We found that the amount of VPS-34 pulled down by anti-FLAG antibodies was significantly lower in *ubc-13(tm3546)* and *chn-1(by155)* than in WT, and the level of VPS-34–associated BEC-1 was also greatly decreased in *ubc-13* and *chn-1* mutants (Fig. 6, A and B). In contrast, the level of BEC-1–MYC pulled down by anti-MYC antibodies was unaffected in *ubc-13(tm3546)* and *chn-1(by155)*, but the level of BEC-1–associated VPS-34 was reduced significantly (Fig. 6, C and D). This suggests that loss of *ubc-13* or *chn-1* affects VPS-34 protein levels. Loss of *ubc-13* or *chn-1* or insertion of a tag into the *vps-34*, *bec-1*, *vps-15*, or *ubq-2* gene locus did not affect *vps-34* mRNA levels (Fig. S4, G–I). Altogether, these data indicate that loss of *ubc-13* and *chn-1* affects the stability of VPS-34 protein, probably through defective ubiquitination of VPS-34. To further test this, we examined VPS-34 levels in *vps-34(qx546)* worms, which carry mutations in the lysine 348 and 352 residues that are important for VPS-34 ubiquitination (Fig. S4 A). We found that the protein level of VPS-34 was significantly reduced in *vps-34(qx546)*, as in *chn-1(by155)*, but

the *vps-34* mRNA level was unaffected (Fig. 6, E and F; and Fig. S4 G). Moreover, VPS-34–associated BEC-1 and VPS-15 were also greatly decreased in *chn-1(by155)* and *vps-34(qx546)* (Fig. 6, E and F). These data indicate that ubiquitin modification of VPS-34 by UBC-13–UEV-1–CHN-1 promotes VPS-34 stability. Consistent with this, overexpression of VPS-34 partially rescued the cell corpse phenotype in *chn-1(by155)* mutants (Fig. S5 D). We found that the level of MYC–VPS-15 pulled down by anti-MYC antibodies was decreased significantly in *chn-1(by155)* and *vps-34(qx546)*, and the level of VPS-15–associated VPS-34 was also reduced (Fig. 6, G and H). In addition, the association of VPS-34 with BEC-1 and VPS-15 was reduced in *chn-1(by155)* and *vps-34(qx546)* mutants (Fig. S5, E and F). These data suggest that defective ubiquitin modification of VPS-34 affects VPS-15 stability and may impair assembly of the VPS-34 complex.

Discussion

Here we report that VPS-34 is modified by K63-linked poly-ubiquitination, and this modification is important for the function of VPS-34 in apoptotic cell clearance. In the ubiquitination process, the E3 ubiquitin ligase CHN-1 interacts through its U-box domain with the E2-conjugating enzyme UBC-13 and through its TPR and helical domains with the C2 domain of VPS-34. CHN-1 thus mediates K63-linked poly-ubiquitination of VPS-34 both in vitro and in *C. elegans*. Mutations in lysine residues 348 and 352 of VPS-34, which are conserved across species from yeast and worms to humans, abolished both mono- and poly-ubiquitination of VPS-34 in vitro and reduced poly-ubiquitination of VPS-34 in worms to a similar level as in *chn-1(lf)* mutants. This suggests that K348 and K352 are the major sites of VPS-34 ubiquitination by UBC-13–UEV-1–CHN-1. The failure to detect K348K352-containing peptides in mass spectrometry analyses may be a result of instability of the peptides. Distinct from ubiquitin-mediated proteasome degradation of VPS34 reported previously in cultured cells (Xiao et al., 2015; Liu et al., 2016), we found that the protein but not the mRNA level of *vps-34* was significantly reduced in *ubc-13(lf)*, *chn-1(lf)*, or *vps-34(qx546)* mutants, which are defective in VPS-34 ubiquitination. This indicates that the K63-linked poly-ubiquitination catalyzed by UBC-13–UEV-1–CHN-1 protects instead of disrupts VPS-34 stability. Consistent with our work, K63-linked ubiquitination has been found to promote ULK-1 stability, self-interaction, and function (Nazio et al., 2013). In this process, AMBRA1 interacts with the E3 ligase TRAF6 to mediate ubiquitin modification of ULK1.

The crystal structure of the yeast Vps34 complex II (Vps34-Vps15-Vps30-Vps38) and single-particle EM of the human VPS34 complex I (VPS34-VPS15-BECN1-ATG14) revealed that Vps34 interacts extensively with Vps15 to form one arm of the Y-shaped complex (Baskaran et al., 2014; Rostislavleva et al., 2015). The C2 domain, which mediates
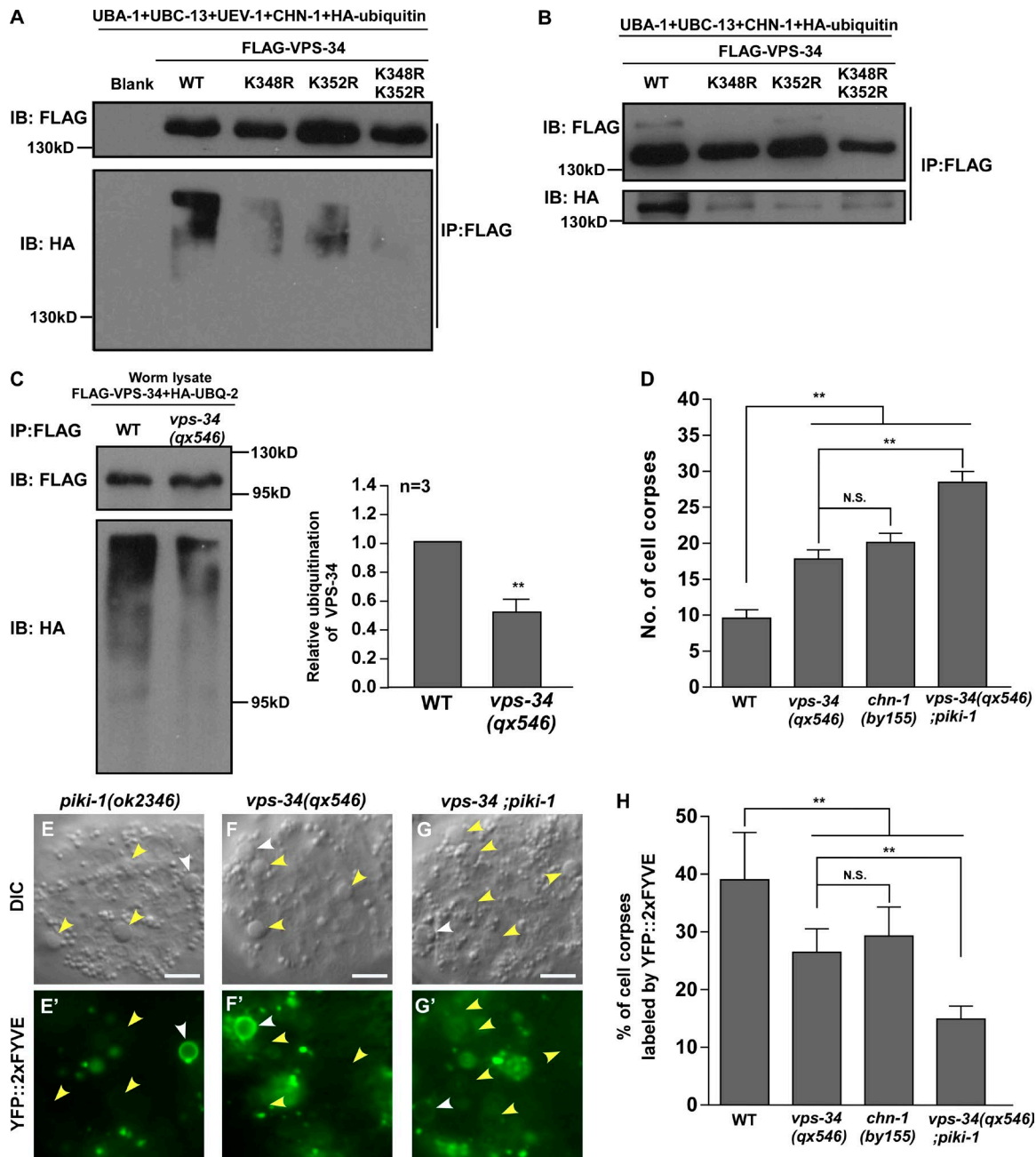

Figure 5. **Lysine residues 348 and 352 are important for the ubiquitination of VPS-34 in vitro and in vivo.** (A and B) Mutations of lysine 348 (K348) and lysine 352 (K352) abrogated poly- (A) and mono (B)-ubiquitination of VPS-34 in vitro. FLAG IP was performed followed by detection of ubiquitination with anti-HA antibodies. (C) Ubiquitination of VPS-34 was examined in WT and *vps-34(qx546)* mutants carrying both *ha::ubq-2* and *flag::vps-34* (WT) or *flag::vps-34 (K348RK352R)* (*vps-34[qx546]*) generated by CRISPR-Cas9. The graph shows quantification of the level of ubiquitination using ImageJ (version 1.48v). The ratio of ubiquitin versus FLAG-VPS-34 was determined and normalized to onefold in WT. At least three independent experiments were performed. Data are shown as mean ± SD and were compared using the unpaired *t* test. **, P < 0.0001. (D) Cell corpses were scored at the twofold embryonic stage in the indicated strains. (E–G′) DIC and fluorescent images of cell corpses in *piki-1(ok2346)*, *vps-34(qx546)*, and *vps-34;piki-1* embryos expressing YFP::2XFYVE. The head region of embryos at the twofold stage is shown. Cell corpses labeled by YFP::2XFYVE are indicated by white arrowheads whereas unlabeled corpses are indicated by yellow arrowheads. (H) The percentage of cell corpses labeled by YFP::2xFYVE in WT, *vps-34(qx546)*, *chn-1(by155)*, and *vps-34(qx546);piki-1* was quantified. In (D and H), at least 15 embryos were scored in each strain and data are shown as mean ± SD. One-way ANOVA with Tukey's posttest was performed to compare datasets linked by lines (D) or mutant datasets with WT (H). **, P < 0.0001; N.S., no significance. Bars, 5 µm.

numerous protein–protein interactions of Vps34, appears to sit at the center of the Y-shaped complex but is remote from the rest of the enzyme (Baskaran et al., 2014; Rostislavleva et al., 2015). We found that CHN-1 associates with the C2 domain of VPS-34 and mediates K63-linked poly-ubiquitination of

VPS-34 at least in part through the lysine residues 348 and 352, which are located in the helical region of the enzyme. Given the high flexibility of the linker region between the C2 and the helical-catalytic domain (Rostislavleva et al., 2015), we hypothesize that the K63-linked ubiquitin modification of VPS-34 may
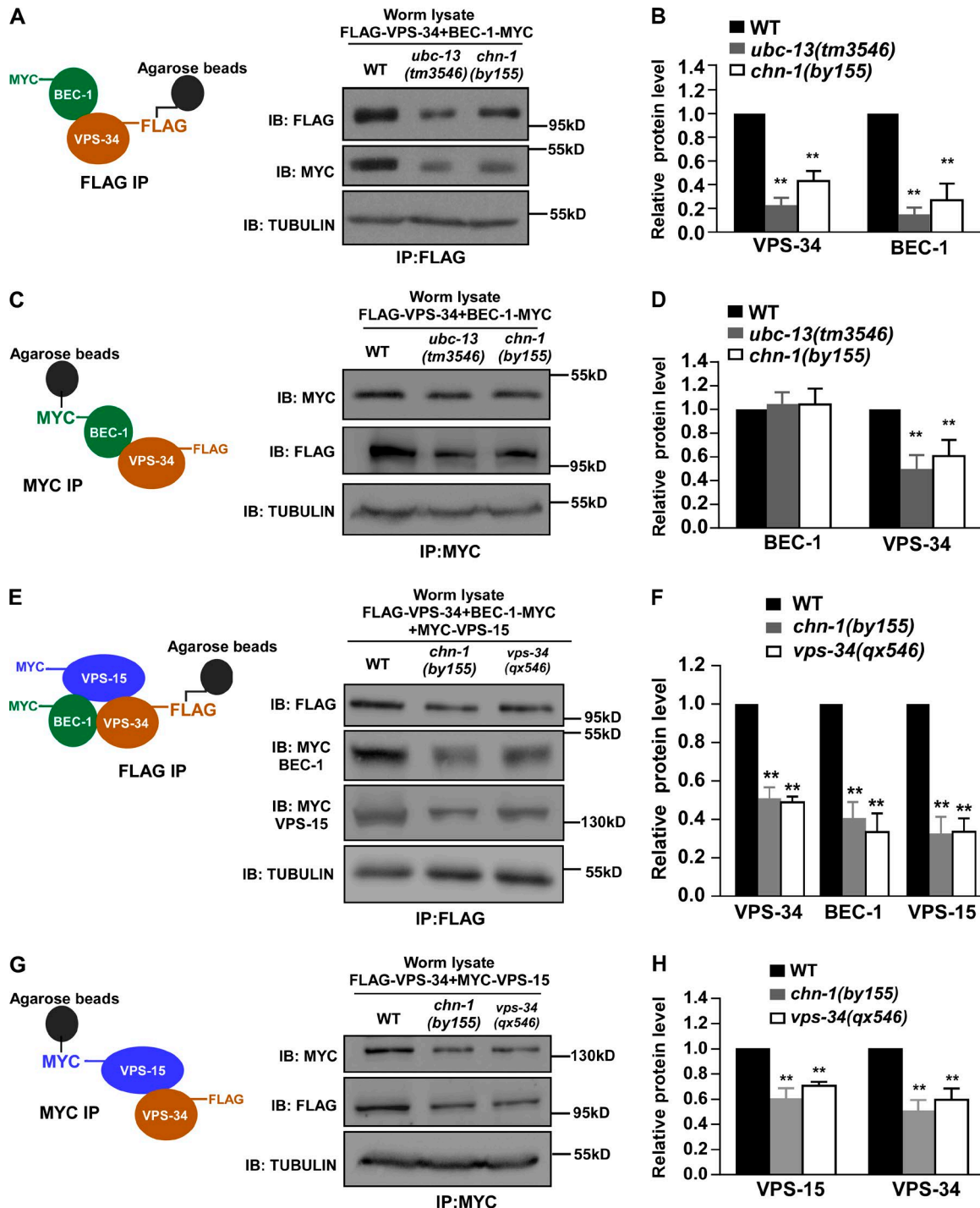
Figure 6. **Loss of UBC-13 and CHN-1 affects protein levels of VPS-34.** Schematic illustration of the IP experiment is shown at the left of panels (A, C, E, and G). Worm lysates were prepared from strains carrying *flag-vps-34* and *bec-1-myc* (A, C), *flag-vps-34*, *bec-1-myc*, and *myc-vps-15* (E) or *flag-vps-34* and *myc-vps-15* (G) generated by CRISPR-Cas9. VPS-34, BEC-1, and VPS-15 were detected by anti-FLAG and anti-MYC antibodies as indicated. Tubulin was the loading control for all blots. The graphs show relative protein levels, which were quantified using ImageJ (B) or ClinX Image Analysis (D, F, and H) as mean ± SD of 3 independent sets of experiments. Mutant datasets were compared with WT using the unpaired *t* test. **, P < 0.0001; all other points have P > 0.05.

induce conformational changes important for VPS-34 stability and/or its association with VPS-15, which may further stabilize VPS-34 and promote complex assembly. We found that VPS-15 protein levels were reduced significantly in animals carrying *chn-1(lf)* and *vps-34(qx546)* mutants, which impair ubiquitination and reduce the stability of VPS-34, suggesting

that VPS-34 is important for VPS-15 stability (Fig. 6, G and H). This is consistent with the finding in yeast that depletion of Vps34 reduces Vps15 levels, and with the structural analyses of Vps34 complexes, which reveal extensive interactions between Vps-34 and Vps-15 (Kihara et al., 2001; Baskaran et al., 2014; Rostislavleva et al., 2015). In contrast, loss of *ubc-13* or *chn-1*

caused a significant reduction in the protein levels of VPS-34 but not BEC-1. Knockdown of VPS34 by siRNA in mammalian cells causes reduced Beclin 1 levels, whereas the cellular level of Vps30 (yeast homologue of Beclin 1) is unaffected in *vps34*-deleted yeast cells (Kihara et al., 2001; Itakura et al., 2008; Thoresen et al., 2010). Differences in the abundance of VPS-34 and BEC-1 proteins in different species or additional regulation of VPS34 complexes in mammalian cells may account for this discrepancy.

In addition to affecting maturation of apoptotic cell–containing phagosomes, loss of UBC-13 and CHN-1 also impairs autophagy, suggesting that the K63-linked ubiquitin modification may serve as a general regulatory mechanism to modulate VPS-34 stability under basal conditions. In *chn-1(lf)*, the effect on phagosomal PtdIns3P is strong, whereas the autophagy phenotypes are relatively mild. This may reflect the different threshold levels of PtdIns3P that are required in different processes. Consistent with this, apoptotic cell clearance but not autophagy is severely affected in *piki-1*–defective worms (Wu et al., 2014).

When expressed in worms, UBE2N/Ubc13, the human homologue of UBC-13, efficiently rescued the cell corpse phenotype in *ubc-13(lf)* mutants, suggesting evolutionarily conserved roles of Ubc13 in this process. Ubc13 is the only E2 that is known to generate K63-linked ubiquitin chains. It plays critical roles in many cellular processes by working with various E3 ubiquitin ligases including CHIP, the human U-box E3 homologous to CHN-1 (Hodge et al., 2016). CHIP functions as both a cochaperone and an E3 ubiquitin ligase to take part in the protein folding–refolding pathway and to mediate degradation of a wide variety of substrates through the proteasomal and autophagy pathways (Edkins, 2015). Our findings reveal a previously unknown function of UBC-13/Ubc13 and CHN-1/CHIP in protecting VPS-34/VPS34 stability, which extends the roles of these two ubiquitinating enzymes in VPS34-controlled PtdIns3P-mediated cellular processes.

Materials and methods

C. elegans strains

Strains of *C. elegans* were cultured and maintained using standard protocols. The N2 Bristol strain was used as the WT strain except for polymorphism mapping, in which Hawaiian strain CB4856 was used. Standard microinjection methods were used to generate transgenic animals carrying extrachromosomal arrays (*qxEx*), and genome-integrated arrays (*qxIs*) were acquired by γ-irradiation to achieve stable expression from arrays with low copy numbers. Strains that were used in this work are summarized in Table S1. The *vps-34*–deficient strain, *vps-34(h797)*, and the *bec-1*–deficient strain, *bec-1(ok700)*, are maintained as *dpy-5(e61)vps-34(h797);qxEx(vps-34*[+];P$_{sur-5}$-SUR-5-GFP) and *bec-1(ok700);qxEx(bec-1*[+];P$_{sur-5}$SUR-5-GFP), respectively. Non-green embryos were scored as *vps-34(lf)* (*dpy-5[e61]vps-34[h797]*) or *bec-1(lf)* (*bec-1[ok700]*). All mutant strains were outcrossed with the WT N2 strains at least 4 times before further analysis. We obtained *ubc-13(tm3546)* and *chn-1(tm2692)* from S. Mitani (Tokyo Women's Medical University, Tokyo, Japan), *smIs34* (P$_{ced-1}$CED-1::GFP) from D. Xue (University of Colorado, Denver, CO), and *opIs334* (P$_{ced-1}$YFP::2xFYVE) from K.S. Ravichandran (University of Virginia, Charlottesville, VA) and M.O. Hengartner (Univerisity of Zurich, Zurich, Switzerland).

Isolation, mapping, and cloning of *ubc-13*

The *qx222* mutation was isolated from a forward genetic screen for animals that contained increased numbers of embryonic cell corpses. *qx222* was mapped to the left arm of linkage group IV (LG IV) between genetic map positions −7.60 and −5.36 by single nucleotide polymorphism mapping. Transformation rescue experiments were performed, and a plasmid containing the *ubc-13* gene rescued the cell corpse phenotype in *qx222*. The sequence of the *ubc-13* gene was determined in *qx222*, which contains a G to A transition that results in a premature stop codon after Val 70. Both *qx222* and the deletion allele *tm3546* are predicted to result in a truncated protein that lacks the catalytic cysteine residue essential for the enzymatic activity of E2, suggesting that they are strong loss-of-function or null alleles of *ubc-13*. *qx222* and *tm3546* were backcrossed with N2 worms six times before further analysis.

Quantification of cell corpses and phagosome maturation

Cell corpses were identified by their raised button–like morphology using Nomarski optics. The number of somatic cell corpses in the head region of living embryos was quantified either at different embryonic stages for time course analysis or at the twofold stage as indicated in the legends of Figs. 1, S1, and S2. At least 15 animals were quantified at each stage in each strain. To examine cell corpse duration, embryos at the precomma stage were mounted on agar pads. Images in 30 z series (1.0 µm/section) were captured every 2 min for 2–4 h using an Axioimager M1 microscope equipped with an AxioCam monochrome digital camera (Carl Zeiss Inc.). Images were processed and viewed using Axiovision Rel 4.7 software.

To examine phagosome maturation, differential interference contrast (DIC) and fluorescence images were captured using an Axioimager A1 microscope (Carl Zeiss Inc.). The total number of cell corpses and the number of cell corpses that were labeled by different phagosomal markers were scored using DIC and fluorescent microscopy. The percentage of cell corpses labeled by phagosomal markers was calculated as (number of labeled cell corpses/total number of corpses) × 100.

Microscopy and imaging analysis

DIC and fluorescent images were captured with an Axioimager A1 equipped with epifluorescence (filter set 13 for GFP [excitation BP 470/20, beam splitter FT 495, and emission BP 503–530]) and an Axio-Cam monochrome digital camera. Images were processed and viewed using Axiovision Rel. 4.7 software (Carl Zeiss Inc.). A 100× objective (Plan-Neofluar; NA1.30) was used with Immersol 518F oil (Carl Zeiss Inc.). All images were taken at 20°C.

Quantification of LGG-1 puncta

To quantify accumulation of LGG-1–positive structures, we generated a single copy insertion reporter of GFP::LGG-1 by CRISPR-Cas9. The number of GFP::LGG-1 puncta was scored at the larvae 1 (L1) stage. Fluorescent images in 40–50 z series (0.5 µm/section) were captured using a 60× objective (CFI Plan Apochromat Lambda; NA 1.45; Nikon) on an inverted fluorescence microscope (Eclipse Ti-E; Nikon) with an UltraView spinning-disc confocal scanner unit (PerkinElmer Inc.) with 488 (emission filter 525 [W50]) laser. Serial optical sections were analyzed, and the number of GFP::LGG-1 puncta was quantified by Volocity software (PerkinElmer Inc.). At least 20 animals were quantified in each strain.

Starvation assay

Embryos were synchronized, collected, and incubated in deionized distilled water at 20°C. At each time point, an aliquot of each sample was placed on an OP50-seeded plate. After 3 d at 20°C, the number of

animals surviving to L4 or adulthood was counted. At least 600 animals were quantified each day.

Yeast two-hybrid analyses

The ProQuest yeast two-hybrid system was used to search for UBC-13–interacting proteins using UBC-13 and UBC-13(C88G) as baits. Yeast two-hybrid analyses were performed according to the manufacturer's instructions (GibcoBRL). In brief, cDNA encoding UBC-13 or the enzymatic dead UBC-13(C88G) was cloned into pDBleu vector, and expression of UBC-13 and UBC-13(C88G) was determined by Western blot analyses. The optimal concentration of 3-amino-1,2,4-triazole was determined by self-activation testing of UBC-13. The *C. elegans* pPC86-library was then screened using pDBleu–UBC-13 and pDBlue–UBC-13 (C88G). Transformants were selected on synthetic complete (SC) medium lacking leucine, tryptophan, and histidine (SC-Leu-Trp-His) with optimal 3-amino-1,2,4-triazole for the activation of the reporter gene *HIS3*. The positive transformations were sequenced to identify the gene.

To examine protein–protein interactions, yeast two-hybrid analyses were performed using the Matchmaker yeast two-hybrid system by following the manufacturer's instructions (Clontech). Specific cDNAs to be tested were cloned into the pGADT7 and pGBKT7 vectors to produce Gal4 transcription activation domain and DNA binding domain fusion proteins. Specific pairs of constructs expressing activation domain and binding domain fusion proteins were transformed into the yeast strain AH109, and transformants were selected on SC medium lacking leucine and tryptophan (SC-Leu-Trp). Individual clones were streaked on SC-Ade-His-Leu-Trp plates to test for the activation of the reporter genes *HIS3* and *ADE2*.

Expression and purification of recombinant proteins

Full-length cDNAs of *ubc-13* (WT/P98GA99G) were cloned into the pET21b (6xHIS tag) and pGEX-6p-1 (GST fusion) vectors. Full-length cDNAs of *C. elegans uba-1*, *uev-1*, and *ubq-2* (ubiquitin region: WT, K63R, and K48R) were cloned into the pET28a vector. cDNAs encoding MYC–CHN-1, FLAG–BEC-1, SMT3–FLAG–VPS-34, TRX–FLAG–VPS-34, or FLAG–VPS-34 (full length, C2 domain, and core domain) were cloned into the pET28a and the pGEX-6p-1 vectors. The recombinant proteins were produced in the *Escherichia coli* BL21 (DE3) strain induced by IPTG at 16°C. The 6xHIS and GST fusion proteins were purified using Ni-NTA resin (Qiagen) and glutathione-sepharose beads (Sigma-Aldrich), respectively.

GST pulldown assay

To investigate the UBC-13–CHN-1 interaction, GST–UBC-13 and GST–UBC-13(P98GA99G) were immobilized on glutathione-sepharose beads and incubated with MYC–CHN-1 (500 ng) for 1 h in a binding buffer containing 25 mM Tris-HCl, pH 7.4, 150 mM NaCl, and 0.5% NP-40. To investigate the CHN-1–VPS-34, CHN-1–BEC-1,

and VPS-34–BEC-1 interactions, GST, GST–CHN-1, and GST–BEC-1 were immobilized on glutathione-sepharose beads and incubated with 800 ng of recombinant SMT3–FLAG–VPS-34, FLAG–VPS-34 (C2), or SMT3–FLAG–VPS-34 (core) for 1 h in the binding buffer. The resins were washed five times in washing buffer containing 25 mM Tris-HCl, pH7.4, 300 mM NaCl, and 0.5% NP-40, and the bound proteins were analyzed by Western blotting.

Ubiquitination assay

To examine ubiquitin modification in vitro, 1 µg WT or mutated forms of SMT3–FLAG–VPS-34, TRX–FLAG–VPS-34, SMT3–FLAG–VPS-34 (core), or FLAG–BEC-1 were incubated with 100 ng E1, 250 ng UBC-13, 250 ng UEV-1, 600 ng CHN-1, and 2 µg HA-ubiquitin (WT, K63R, or K48R) in ubiquitin ligation buffer containing 25 mM Tris-HCl (pH7.4), 100 mM NaCl, 10 mM MgCl$_2$, 2 mM ATP, and 0.5 mM DTT at 20°C for 2 h. The reaction was terminated by boiling for 5 min in SDS sample buffer and analyzed by Western blotting.

To analyze ubiquitination of VPS-34 in vivo, mix-staged worms carrying *flag–vps-34* and *ha–ubq-2* generated by CRISPR-Cas9 were collected and washed in M9 buffer, then frozen in liquid nitrogen with lysis buffer containing 25 mM Tris-HCl, pH 7.4, 150 mM NaCl, 1% NP-40, and protease inhibitor cocktail. The worms were homogenized completely with tissue grinders, then centrifuged at 3,500 *g* for 30 min to remove debris. The resulting worm lysates were incubated with anti-FLAG M2 beads (Sigma-Aldrich) overnight. After extensive washing with lysis buffer, the bound proteins were resolved with SDS-PAGE and revealed by Western blotting with antibodies against FLAG (rabbit; Sigma-Aldrich) and HA (Sigma-Aldrich).

Coimmunoprecipitation assay in worms

Worms carrying *flag–vps-34* and/or *bec–1-myc* and/or *myc–vps-15* generated by CRISPR-Cas9 were harvested and frozen in liquid nitrogen with lysis buffer containing 25 mM Tris-HCl, pH 7.4, 150 mM NaCl, 1% NP-40, and protease inhibitor cocktail. The worms were homogenized completely with tissue grinders. FLAG–VPS-34 was immunoprecipitated with anti-FLAG M2 beads (Sigma-Aldrich), whereas BEC–1-MYC and MYC–VPS-15 were immunoprecipitated with anti-MYC agarose (Thermo Fisher Scientific). The bound proteins were washed five times with lysis buffer, resolved with SDS-PAGE, and revealed by Western blotting with antibodies against FLAG (rabbit; Sigma-Aldrich) and MYC (rabbit; Santa Cruz).

Mutagenesis and generation of knock-in worms using CRISPR-Cas9

The site-directed mutagenesis and insertion of tags at specific sites by CRISPR-Cas9 was performed as described before (Paix et al., 2014). In brief, single guide RNA (sgRNA) sites in the targeted gene were chosen using the CRISPR design tool from Feng Zhang's laboratory (http://crispr.mit.edu/). The specific sgRNA sites were introduced into the vector (pDD162-P$_{eft-3}$::CAS9-P$_{u6}$::sgRNA), which expresses CAS9

Table 1. **The guide sequences used for gene editing by CRISPR-Cas9**

Gene	CRISPR-Cas9 targets (PAM)	Allele
vps-34	5′-**CCA**GGTATGCGGGCGACACCGAC-3′	qx477
	5′-ACCTGTTCAGATATGATTCC**AGG**-3′	qx467
	5′-ATATCTACGATCAGTTAATT**GGG**-3′	qx456
bec-1	5′-ATCCCGTGAAATCACTAAAT**AGG**-3′	qx512
ubq-2	5′-AATCTTCGTCAAGACTCTGA**CGG**-3′	qx473
vps-15	5′-ACTTTTCACAACGAATCCGT**CGG**-3′	qx523
	5′-CTCGTCTCTTCTGGCTACGA**TGG**-3′	qx525

The protospacer adjacent motif (PAM) sites are in bold.

enzyme and sgRNA. Single-strand oligodeoxynucleotides were used as the homology-directed repair templates with 30–50 nt homologous arms and optimal restriction enzyme sites. *dpy-10* was used as the positive selection marker as reported previously (Paix et al., 2014). F1 worms that were either dumpy or roller were picked out and screened for recombination by PCR and restriction enzyme digestion. The recombinants were sequenced to confirm homology-directed repair that occurred correctly as designed. The GFP::LGG-1 reporter was generated by inserting *gfp::lgg-1* as a single copy at the Mos1 site on LG IV by CRISPR-Cas9 as described before (Takayanagi-Kiya et al., 2016). In brief, the *P_{lgg-1}gfp::lgg-1::lgg-1 3′UTR* DNA cassette was inserted between the homology arms in donor vectors containing the hygromycin resistance gene. Antibiotic hygromycin B was used as the positive selection drug and *P_{myo-3}::gfp* was used as the negative selection marker. The recombinants were sequenced to confirm that single-copy insertion had occurred correctly as designed.

All strains were backcrossed with WT N2 animals at least four times before further analyses.

The guide sequences used for gene editing by CRISPR-Cas9 are in shown in Table 1.

Analysis of *vps-34* expression by Q-PCR

Total RNA was extracted from well-fed worms using Trizol reagent (Invitrogen), and contaminating DNA was removed by DNase. 500 ng of total RNA was used for reverse transcription with oligo dT as primers. The reverse transcription products (cDNA) were diluted (1:5), and 2 µl of the diluted cDNA was used as the template for quantitative PCR in a 20-µl reaction mixture. For quantitative RT-PCR, FastStart Universal SYBR Green Master (Roche) was used on an Applied Biosystems QuantStudio 7 Flex real-time PCR system. The gene *act-1* was used as the internal reference. At least three independent repeats were done with 3 replications each time. The primers used for the quantitative PCR were as follows: *act-1*, forward primer, 5′-ATATGCCCTCCC ACACGCCA-3′; reverse primer, 5′-AGCGGCGGTGGCCATTTCTT-3′; *vps-34*, forward primer, 5′-GTCGATTCTGCCTACCGGAT-3′; reverse primer, 5′-GGAGGCGTTGTTCGATCTTG-3′.

Mass spectrometric analysis

Protein bands on the SDS-PAGE gel were destained, and then reduced in 10 mM DTT at 56°C for 30 min followed by alkylation in 55 mM iodoacetamide for 1 h in the dark. After that, the protein bands were in-gel digested with sequencing grade trypsin (10 ng/µl trypsin and 50 mM ammonium bicarbonate, pH 8.0) overnight at 37°C. Peptides were extracted with 5% formic acid/50% acetonitrile and 0.1% formic acid/75% acetonitrile sequentially and then concentrated to ∼20 µl. The extracted peptides were separated on an analytical capillary column (50 µm × 15 cm) packed with 5 µm spherical C18 reverse-phase material (YMC). A nanoAcquity UPLC system (Waters) was used to generate the following HPLC gradient: 0–30% B in 40 min and 30–70% B in 15 min (A = 0.1% formic acid in water and B = 0.1% formic acid in acetonitrile). The eluted peptides were sprayed into a LTQ Orbitrap Velos mass spectrometer (Thermo Fisher Scientific) equipped with a nano–electrospray ionization ion source. The mass spectrometer was operated in data-dependent mode with one mass spectrometric analysis (MS) scan followed by four collision-induced dissociation and four high-energy collisional dissociation tandem mass spectrometry scans for each cycle. Database searches were performed on an in-house Mascot server (Matrix Science Ltd.) against the VPS-34 protein sequence. The search parameters were 7 ppm mass tolerance for precursor ions and 0.5 D mass tolerance for product ions. In addition, three missed cleavage sites were allowed for trypsin digestion, and the following variable modifications were included: oxidation of methionine, carbamidomethylation of cysteine, and ubiquitination

(glycine-glycine) of lysine. The tandem mass spectra of matched ubiquitinated peptides were manually checked for their validity.

Statistical analysis

The SD was used as y-axis error bars for bar charts plotted from the mean value of the data. Data derived from different genetic backgrounds were compared by Student's two-tailed unpaired *t* test, one-way ANOVA followed by Tukey's posttest, two-way ANOVA followed by Bonferroni posttest, or the Kaplan-Meier method followed by the log-rank test as indicated in the figure legends. Data were considered statistically different at P < 0.05. P < 0.05 is indicated with single asterisks and P < 0.0001 with double asterisks (0.001 in a two-way ANOVA analysis).

Online supplemental material

Fig. S1 shows that *qx222* affects the *ubc-13* gene. Fig. S2 shows that *ubc-13*, *uev-1*, and *chn-1* act in the same pathway with *vps-34* but in parallel to *piki-1* to promote cell corpse removal. Fig. S3 shows that loss of *ubc-13* and *chn-1* partially impairs autophagy. Fig. S4 shows mutation and tag insertion alleles of *vps-34*, *bec-1*, *vps-15*, and *ubq-2* generated by CRISPR-Cas9. Fig. S5 shows that lysine residues 348 and 352 are important for the ubiquitination of VPS-34. Table S1 summarizes strains that were used in this work.

References

Backer, J.M. 2016. The intricate regulation and complex functions of the Class III phosphoinositide 3-kinase Vps34. *Biochem. J.* 473:2251–2271. https://doi.org/10.1042/BCJ20160170

Baskaran, S., L.A. Carlson, G. Stjepanovic, L.N. Young, D.J. Kim, P. Grob, R.E. Stanley, E. Nogales, and J.H. Hurley. 2014. Architecture and dynamics of the autophagic phosphatidylinositol 3-kinase complex. *eLife.* 3:e05115. https://doi.org/10.7554/eLife.05115

Campbell, S.J., R.A. Edwards, C.C. Leung, D. Neculai, C.D. Hodge, S. Dhe-Paganon, and J.N. Glover. 2012. Molecular insights into the function of RING finger (RNF)-containing proteins hRNF8 and hRNF168 in Ubc13/Mms2-dependent ubiquitylation. *J. Biol. Chem.* 287:23900–23910. https://doi.org/10.1074/jbc.M112.359653

Chen, D., H. Xiao, K. Zhang, B. Wang, Z. Gao, Y. Jian, X. Qi, J. Sun, L. Miao, and C. Yang. 2010. Retromer is required for apoptotic cell clearance by

phagocytic receptor recycling. *Science.* 327:1261–1264. https://doi.org/10.1126/science.1184840

Cheng, S., Y. Wu, Q. Lu, J. Yan, H. Zhang, and X. Wang. 2013. Autophagy genes coordinate with the class II PI/PtdIns 3-kinase PIKI-1 to regulate apoptotic cell clearance in C. elegans. *Autophagy.* 9:2022–2032. https://doi.org/10.4161/auto.26323

Cheng, S., K. Wang, W. Zou, R. Miao, Y. Huang, H. Wang, and X. Wang. 2015. PtdIns(4,5)P$_2$ and PtdIns3P coordinate to regulate phagosomal sealing for apoptotic cell clearance. *J. Cell Biol.* 210:485–502. https://doi.org/10.1083/jcb.201501038

Edkins, A.L. 2015. CHIP: a co-chaperone for degradation by the proteasome. *Subcell. Biochem.* 78:219–242. https://doi.org/10.1007/978-3-319-11731-7_11

Hodge, C.D., L. Spyracopoulos, and J.N. Glover. 2016. Ubc13: the Lys63 ubiquitin chain building machine. *Oncotarget.* 7:64471–64504. https://doi.org/10.18632/oncotarget.10948

Hoppe, T., G. Cassata, J.M. Barral, W. Springer, A.H. Hutagalung, H.F. Epstein, and R. Baumeister. 2004. Regulation of the myosin-directed chaperone UNC-45 by a novel E3/E4-multiubiquitylation complex in C. elegans. *Cell.* 118:337–349. https://doi.org/10.1016/j.cell.2004.07.014

Itakura, E., C. Kishi, K. Inoue, and N. Mizushima. 2008. Beclin 1 forms two distinct phosphatidylinositol 3-kinase complexes with mammalian Atg14 and UVRAG. *Mol. Biol. Cell.* 19:5360–5372. https://doi.org/10.1091/mbc.E08-01-0080

Kihara, A., T. Noda, N. Ishihara, and Y. Ohsumi. 2001. Two distinct Vps34 phosphatidylinositol 3-kinase complexes function in autophagy and carboxypeptidase Y sorting in *Saccharomyces cerevisiae*. *J. Cell Biol.* 152:519–530. https://doi.org/10.1083/jcb.152.3.519

Kovacs, A.L., and H. Zhang. 2010. Role of autophagy in Caenorhabditis elegans. *FEBS Lett.* 584:1335–1341. https://doi.org/10.1016/j.febslet.2010.02.002

Liu, C.C., Y.C. Lin, Y.H. Chen, C.M. Chen, L.Y. Pang, H.A. Chen, P.R. Wu, M.Y. Lin, S.T. Jiang, T.F. Tsai, and R.H. Chen. 2016. Cul3-KLHL20 Ubiquitin Ligase Governs the Turnover of ULK1 and VPS34 Complexes to Control Autophagy Termination. *Mol. Cell.* 61:84–97. https://doi.org/10.1016/j.molcel.2015.11.001

Lu, N., Q. Shen, T.R. Mahoney, L.J. Neukomm, Y. Wang, and Z. Zhou. 2012. Two PI 3-kinases and one PI 3-phosphatase together establish the cyclic waves of phagosomal PtdIns(3)P critical for the degradation of apoptotic cells. *PLoS Biol.* 10:e1001245. https://doi.org/10.1371/journal.pbio.1001245

Lu, Q., P. Yang, X. Huang, W. Hu, B. Guo, F. Wu, L. Lin, A.L. Kovács, L. Yu, and H. Zhang. 2011. The WD40 repeat PtdIns(3)P-binding protein EPG-6 regulates progression of omegasomes to autophagosomes. *Dev. Cell.* 21:343–357. https://doi.org/10.1016/j.devcel.2011.06.024

Nazio, F., F. Strappazzon, M. Antonioli, P. Bielli, V. Cianfanelli, M. Bordi, C. Gretzmeier, J. Dengjel, M. Piacentini, G.M. Fimia, and F. Cecconi. 2013. mTOR inhibits autophagy by controlling ULK1 ubiquitylation, self-association and function through AMBRA1 and TRAF6. *Nat. Cell Biol.* 15:406–416. https://doi.org/10.1038/ncb2708

Paix, A., Y. Wang, H.E. Smith, C.Y. Lee, D. Calidas, T. Lu, J. Smith, H. Schmidt, M.W. Krause, and G. Seydoux. 2014. Scalable and versatile genome editing using linear DNAs with microhomology to Cas9 Sites in Caenorhabditis elegans. *Genetics.* 198:1347–1356. https://doi.org/10.1534/genetics.114.170423

Pinto, S.M., and M.O. Hengartner. 2012. Cleaning up the mess: cell corpse clearance in Caenorhabditis elegans. *Curr. Opin. Cell Biol.* 24:881–888. https://doi.org/10.1016/j.ceb.2012.11.002

Reidick, C., F. El Magraoui, H.E. Meyer, H. Stenmark, and H.W. Platta. 2014. Regulation of the Tumor-Suppressor Function of the Class III Phosphatidylinositol 3-Kinase Complex by Ubiquitin and SUMO. *Cancers (Basel).* 7:1–29. https://doi.org/10.3390/cancers7010001

Rostislavleva, K., N. Soler, Y. Ohashi, L. Zhang, E. Pardon, J.E. Burke, G.R. Masson, C. Johnson, J. Steyaert, N.T. Ktistakis, and R.L. Williams. 2015. Structure and flexibility of the endosomal Vps34 complex reveals the basis of its function on membranes. *Science.* 350:aac7365. https://doi.org/10.1126/science.aac7365

Sato, M., R. Konuma, K. Sato, K. Tomura, and K. Sato. 2014. Fertilization-induced K63-linked ubiquitylation mediates clearance of maternal membrane proteins. *Development.* 141:1324–1331. https://doi.org/10.1242/dev.103044

Slotman, J.A., A.C. da Silva Almeida, G.C. Hassink, R.H. van de Ven, P. van Kerkhof, H.J. Kuiken, and G.J. Strous. 2012. Ubc13 and COOH terminus of Hsp70-interacting protein (CHIP) are required for growth hormone receptor endocytosis. *J. Biol. Chem.* 287:15533–15543. https://doi.org/10.1074/jbc.M111.302521

Takayanagi-Kiya, S., K. Zhou, and Y. Jin. 2016. Release-dependent feedback inhibition by a presynaptically localized ligand-gated anion channel. *eLife.* 5:5e21734. https://doi.org/10.7554/eLife.21734

Thoresen, S.B., N.M. Pedersen, K. Liestøl, and H. Stenmark. 2010. A phosphatidylinositol 3-kinase class III sub-complex containing VPS15, VPS34, Beclin 1, UVRAG and BIF-1 regulates cytokinesis and degradative endocytic traffic. *Exp. Cell Res.* 316:3368–3378. https://doi.org/10.1016/j.yexcr.2010.07.008

Tian, Y., Z. Li, W. Hu, H. Ren, E. Tian, Y. Zhao, Q. Lu, X. Huang, P. Yang, X. Li, et al. 2010. C. elegans screen identifies autophagy genes specific to multicellular organisms. *Cell.* 141:1042–1055. https://doi.org/10.1016/j.cell.2010.04.034

Wang, X., and C. Yang. 2016. Programmed cell death and clearance of cell corpses in Caenorhabditis elegans. *Cell. Mol. Life Sci.* 73:2221–2236. https://doi.org/10.1007/s00018-016-2196-z

Wu, Y., S. Cheng, H. Zhao, W. Zou, S. Yoshina, S. Mitani, H. Zhang, and X. Wang. 2014. PI3P phosphatase activity is required for autophagosome maturation and autolysosome formation. *EMBO Rep.* 15:973–981. https://doi.org/10.15252/embr.201438618

Xiao, J., T. Zhang, D. Xu, H. Wang, Y. Cai, T. Jin, M. Liu, M. Jin, K. Wu, and J. Yuan. 2015. FBXL20-mediated Vps34 ubiquitination as a p53 controlled checkpoint in regulating autophagy and receptor degradation. *Genes Dev.* 29:184–196. https://doi.org/10.1101/gad.252528.114

Zou, W., Q. Lu, D. Zhao, W. Li, J. Mapes, Y. Xie, and X. Wang. 2009. Caenorhabditis elegans myotubularin MTM-1 negatively regulates the engulfment of apoptotic cells. *PLoS Genet.* 5:e1000679. https://doi.org/10.1371/journal.pgen.1000679